Missouri S&T Library and Learning Resources

Scholars' Mine

Masters Theses

Student Theses and Dissertations

Summer 2021

Transfer function measurement for automotive intentional EMI and thermal runaway investigation of lithium-ion battery by intentional EMI

Woncheol Song

Follow this and additional works at: https://scholarsmine.mst.edu/masters_theses

 Part of the Electrical and Computer Engineering Commons

Department:

Recommended Citation

Song, Woncheol, "Transfer function measurement for automotive intentional EMI and thermal runaway investigation of lithium-ion battery by intentional EMI" (2021). *Masters Theses*. 8000.
https://scholarsmine.mst.edu/masters_theses/8000

This thesis is brought to you by Scholars' Mine, a service of the Missouri S&T Library and Learning Resources. This work is protected by U. S. Copyright Law. Unauthorized use including reproduction for redistribution requires the permission of the copyright holder. For more information, please contact scholarsmine@mst.edu.

TRANSFER FUNCTION MEASUREMENT FOR AUTOMOTIVE INTENTIONAL EMI AND THERMAL RUNAWAY INVESTIGATION OF LITHIUM-ION BATTERY BY INTENTIONAL EMI

by

WONCHEOL SONG

A THESIS

Presented to the Graduate Faculty of the

MISSOURI UNIVERSITY OF SCIENCE AND TECHNOLOGY

In Partial Fulfillment of the Requirements for the Degree

MASTER OF SCIENCE

in

ELECTRICAL ENGINEERING

2021

Approved by:

Chulsoon Hwang, Advisor
Jun Fan
Daryl G. Beetner

© 2021

Woncheol Song

All Rights Reserved

PUBLICATION THESIS OPTION

This thesis consists of the following two articles, formatted in the style used by the Missouri University of Science and Technology:

Paper I, found on pages 3–20, has been published in *2020 IEEE International Symposium on Electromagnetic Compatibility & Signal/Power Integrity(EMCSI)*, July 2020.

Paper II, found on pages 21–35, is intended for submission to *2022 IEEE International Symposium on Electromagnetic Compatibility & Signal/Power Integrity(EMCSI)*, August 2022.

ABSTRACT

With an increasing demand for electric vehicles and autonomous driving, many components of a vehicle are being replaced as electric components. This implicates the possibility of an increase in the malfunction of electric components due to unknown electromagnetic interferences. In this reason, malicious intentional electromagnetic interference (IEMI) is being considered as a growing threat for the current and next generation of automotive technology.

In the first topic, the transfer function between the IEMI attacker and the engine control unit (ECU) circuit in an automobile is extracted to analyze how the IEMI affects the vehicle.

In the second topic, to mimic the electromagnetic environment which can affect the battery system with inducing a current passing through the battery, the current is intentionally injected to the battery system with a bulk current injection (BCI) probe and it is investigated that how this coupled current can affect the battery with the parallel LC resonance of which the inductance comes from the wire and the capacitance comes from the bypass capacitor before voltage regulator module (VRM).

ACKNOWLEDGMENTS

First of all, I would like to thank my advisor, Prof. Chulsoon Hwang, who helps me to do research topics and projects on the right way. Without his guidance and support, it is impossible to finish my master program. I owe a deep gratitude to him.

Besides my advisor, my committee members, Prof. Jun Fan and Prof. Daryl G. Beetner gave me a lot of help in my study and research. Participating in Dr. Fan's group meeting broadened my view and learned a lot from his comments. From Dr. Beetner's well organized Interference Control course, I could understand why we need study EMC.

Also, I would like to thank all EMC lab faculties and students for all their help. Especially for students at EMC lab, I want to say thank everyone and it has been a great opportunity to know each other and hope to meet everyone again.

Finally, I wish to thank my wife, Minji Yoo, my daughter, Hayun Song, and my parents who care and love me most. Without their support, I couldn't finish my study.

Many thanks and best wishes to everyone in the EMC Laboratory!

TABLE OF CONTENTS

LIST OF ILLUSTRATIONS

PAPER I Page

PAPER II

LIST OF TABLES

PAPER II Page

SECTION

1. INTRODUCTION

1.1. BACKGROUND

With an increasing demand for electric vehicles and autonomous driving, many components of a vehicle are being replaced as electric components. This implicates the possibility of an increase in the malfunction of electric components due to unknown electromagnetic interferences. In this reason, malicious IEMI is being considered as a growing threat for the current and next generation of automotive technology. It works by intentionally inducing noise, thereby disrupting the normal operation of a system. This issue emphasizes the importance of understanding potential risks that this intentional threat will cause.

Lithium-Ion (Li-ion) batteries are being widely used nowadays for electric vehicles and electric devices and the demand of Li-ion batteries is rapidly increasing. However, many accidents related with Li-ion batteries also have been reported recently. Most of solutions of the thermal runaway of Li-ion batteries are focused on the battery itself. Considering the transfer function, we can calculate how much the field is radiated from the noise source to the victim and RF current can be induced with radiated fields. It is found that due to the bypass capacitor and the inductance of the wire at the battery, the parallel LC resonance is generated and the induced current from the noise source is resonated with this resonance and when it passes through the battery, it can generate a thermal runaway of the battery.

1.2. CONTENTS

This thesis consists of two papers. The first paper is related to the transfer function measurement for automotive intentional EMI and the second paper is related to the thermal runaway investigation of lithium-ion battery by intentional EMI.

PAPER

I. TRANSFER FUNCTION MEASUREMENT FOR AUTOMOTIVE INTENTIONAL ELECTROMAGNETIC INTERFERENCE

Woncheol Song, Yang Zhong, Cheolhan Kim, Changyul Park, and Chulsoon Hwang

ABSTRACT

The transfer function between the intentional electromagnetic interference (IEMI) attacker and the engine control unit (ECU) circuit in an automobile is extracted to analyze how the IEMI affects the vehicle. A log-periodic antenna is used as the IEMI aggressor based on the frequency domain measurement and the transfer function of the log-periodic antenna is compared with the transfer function of the standard mesoband source generator measured in the time domain. The electric field of the standard source is regenerated with the transfer function of the log-periodic antenna. It is then compared with the original field of the standard source to validate the transfer function of the log-periodic antenna. Since the D-dot sensor is used to measure radiated field in the time domain, a noise in low frequency region is amplified and it is investigated.

1. INTRODUCTION

With an increasing demand for electric vehicles and autonomous driving, many components of a vehicle are being replaced as electric components. This implicates the

possibility of an increase in the malfunction of electric components due to unknown electromagnetic interferences. As an example, when antilock braking system (ABS) was first introduced, braking problems arose on the German autobahn when vehicles passed a nearby radio transmitter [1]. Malicious IEMI is being considered as a growing threat for the current and next generation of automotive technology. It works by intentionally inducing noise, thereby disrupting the normal operation of a system. This issue emphasizes the importance of understanding potential risks that this intentional threat will cause.

Several experiments were conducted to understand automotive IEMI [2-4]. They were based on the time domain measurement and a D-dot sensor was used to measure the radiated electric field [5]. Due to the characteristics of a D-dot sensor, the low frequency noise is amplified with the time domain measurement and it occurs the uncertainty of the measurement. Also, standard IEMI source generators are usually required to analyze automotive IEMI [6]. However, experiments using these source generators were costly and dangerous, since they are huge and generate high power electromagnetic (HPEM) fields of tens or hundreds of kV/m at peak field strengths. This facilitates the need to test the IEMI using an alternative aggressor other than standard IEMI attackers.

In this paper, the transfer function between the IEMI source and the ECU circuit in the automobile is extracted to analyze how IEMI affects the vehicle and the low frequency noise with the time domain measurement is investigated. Instead of standard IEMI sources, the log-periodic antenna is used as an aggressor and the measurement is conducted in the frequency domain. A transfer function of a system is a ratio of the output to the input of the system and it is used to describe and analyze the system in the

frequency domain. To offset the effect using different IEMI sources, a transfer function is considered to show how a radiated electric field affects the vehicle; therefore, vulnerable frequencies can be specified. It is calculated with reconstructed dipole moments of the log-periodic antenna and compared with the transfer function of the standard mesoband source measured in the time domain. To validate if the transfer function of the log-periodic antenna is comparable to the standard source generator, the electric field of the standard source is regenerated with the transfer function of the log-periodic antenna and is compared with the original standard source field waveform.

2. IEMI SOURCE CHARACTERIZATION

To calculate the transfer function, the system's input and output need to be well defined. In [2], the mesoband standard source generator was used as Figure 1 to reconstruct the IEMI source for the numerical simulation. Since the generator is based on the dipole antenna structure, the dominant current flows in the vertical direction through dipole arms; therefore, the Hertzian dipole is considered for the source reconstruction. Also, the transverse electromagnetic (TEM) sensor is placed at a height similar to that of the center of the standard source to measure the radiated field from the generator. In this case, the dominant field's component is in the vertical direction. The dipole moment of the aggressor P_z and its radiated electric field E_z to the victim are considered as the input and output to extract the transfer function for IEMI analysis.

(a) The setup for the source reconstruction

(b) IEMI measurement setup

Figure 1. The mesoband standard source measurement setup

In this section, IEMI dipole moments P_z was reconstructed by the source reconstruction using the log-periodic antenna. Also, radiated electric fields E_z from the log-periodic antenna were measured using a D-dot sensor. With these values, the transfer function of the log-periodic antenna is calculated and compared with the standard source.

To validate if the transfer function of the log-periodic antenna is comparable to the standard source, the electric field is regenerated as the transfer function of the log-

periodic antenna multiplied by dipole moments of the standard source and compared with the original electric field radiated from the standard source.

2.1. MEASUREMENT FOR IEMI SOURCE MODELING

The measurement setup with the log-periodic antenna is illustrated in Figure 2.

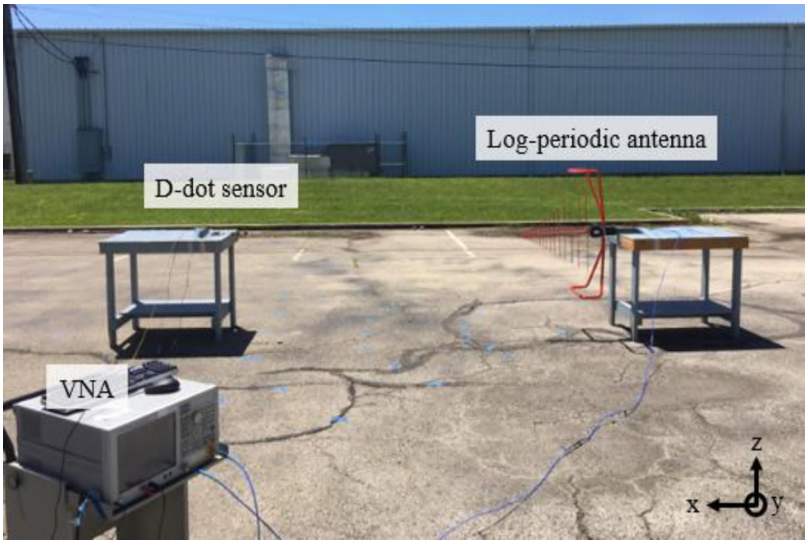

(a) Measurement setup for the source reconstruction

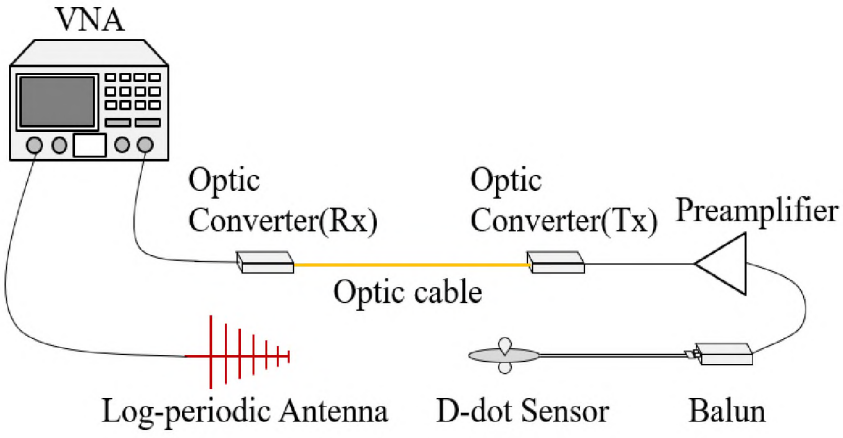

(b) Measurement setup illustration

Figure 2. The measurement setup for IEMI source modeling

The log-periodic antenna was used as an IEMI source. The free-field D-dot sensor and the log-periodic antenna are placed at z = 1 m. The preamplifier is a low noise amplifier (LNA) to improve the signal-to-noise ratio (SNR).

In the far-field region, it is reasonable to replace the source with an ideal infinitesimal electric dipole. Based on the log-periodic antenna structure with a height of 0.74 m, the far-field boundary can be estimated as 1.825 m at 500 MHz by the following Equation (1) [7]:

$$R = \frac{2D^2}{\lambda} = \frac{2(0.74\,m)^2}{\frac{3}{5}m} \approx 1.825\,m, \tag{1}$$

where D is the largest dimension of the antenna, and λ is the wavelength of the signal in the air at 500 MHz.

The D-dot sensor was used to measure the radiated electric field. Since it is mounted on a small ground plane, it can be placed in the vehicle where it will measure a surface electric field quantity. The z-components of electric fields were measured at different observation points from 2 m to 6 m which are the distances between the log-periodic antenna's calibration reference point and the D-dot sensor. The output of the D-dot sensor is proportional to a time derivative of the electric field; it is proportional to the frequency by Fourier transform. The electric field $E_z(f)$ can be calculated as Equation (2):

$$E_z(f) = \frac{V(f)}{A_{eq}R_0 \times j2\pi f\varepsilon_0} \tag{2}$$

where $V(f)$ is the output voltage of the D-dot sensor in the frequency domain, A_{eq} indicates the equivalent area of the D-dot sensor, R_0 is the characteristic impedance of the

D-dot sensor and ε_0 is the permittivity of free space. Figure 3 shows measured electric fields E_z converted by (2).

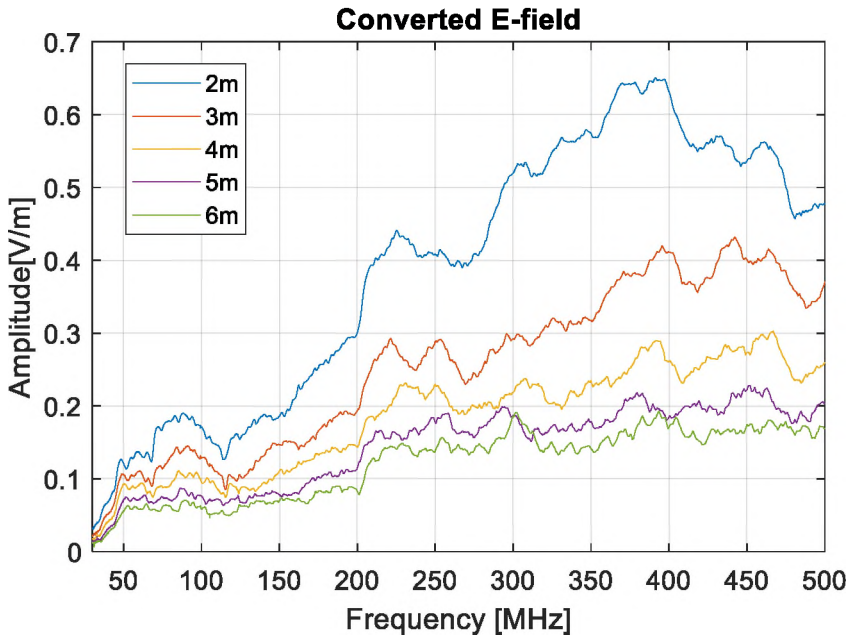

Figure 3. Electric field E_z measurement data

2.2. IEMI SOURCE RECONSTRUCTION

With measured field data, the equivalent dipole moment P_z of the log-periodic antenna was reconstructed by the source reconstruction and the least square method [8, 9]. Since the log-periodic antenna supports above 30 MHz based on the datasheet and the far-field boundary estimation calculated as (1) can be considered below 500 MHz, the dipole moment is reconstructed from 30 MHz to 500 MHz with the step of 10 MHz. Figure 4 shows reconstructed dipoles $P_z(f)$ of the log-periodic antenna. It correlates the antenna factor of the log-periodic antenna on the datasheet especially at a peak near 50 MHz region.

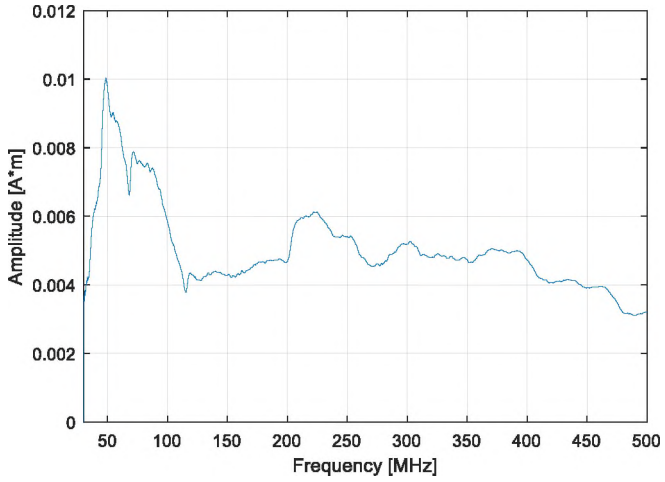

Figure 4. The equivalent dipole moment $P_z(f)$ of the log-periodic antenna

To validate reconstructed dipole moments, the dipole moments are imported on the simulation. The equivalent dipole is placed at z = 1 m which is the same height as the log-periodic antenna placement. Figure 5 compares measurement and simulation results at the point located 2 m away from the source. The simulation result matches well with

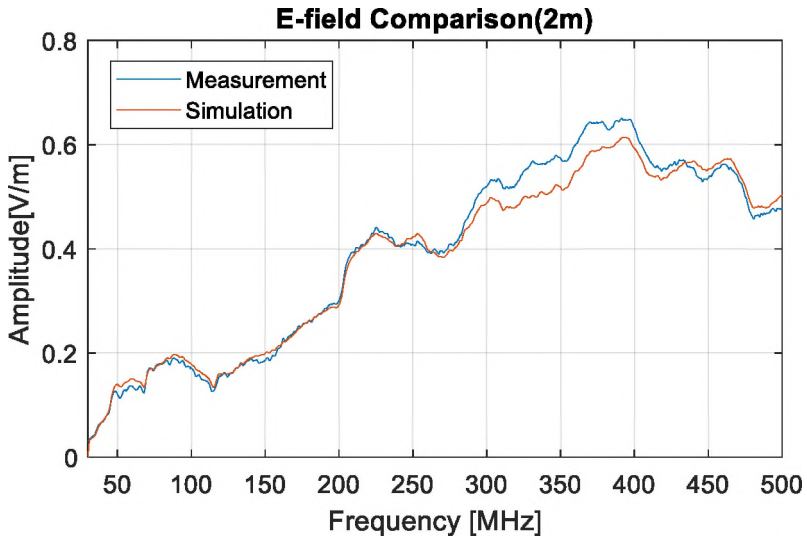

Figure 5. Electric field comparison at 2 m away from the source

the measurement. The reconstructed source generates the same field as the log-periodic antenna does. Also, the data from 3 m to 6 m away from the log-periodic antenna matched well.

2.3. VALIDATION OF THE TRANSFER FUNCTION

The transfer function of the log-periodic antenna can be calculated as Equation (3) shown below:

$$TF(f) = \frac{E_z(f)}{P_z(f)}. \tag{3}$$

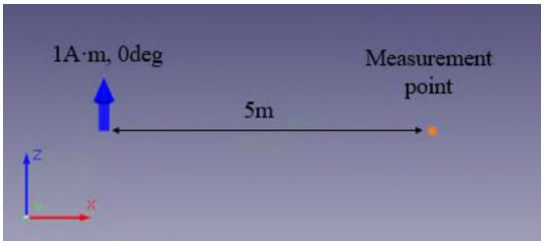

Figure 6. Simulation setup for the transfer function of the unit dipole

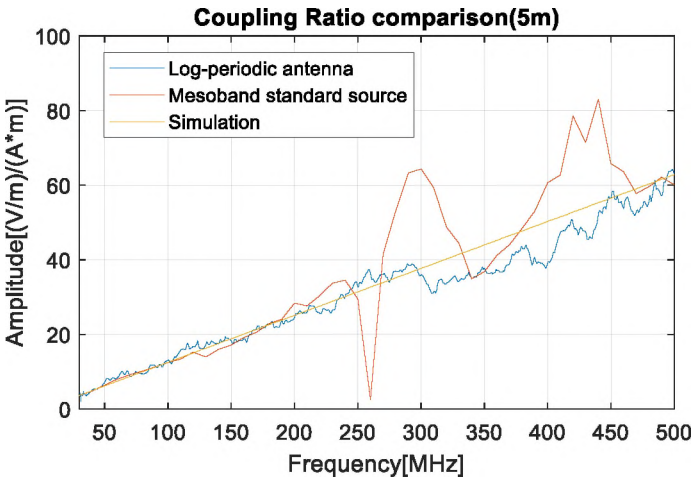

Figure 7. Transfer function comparison

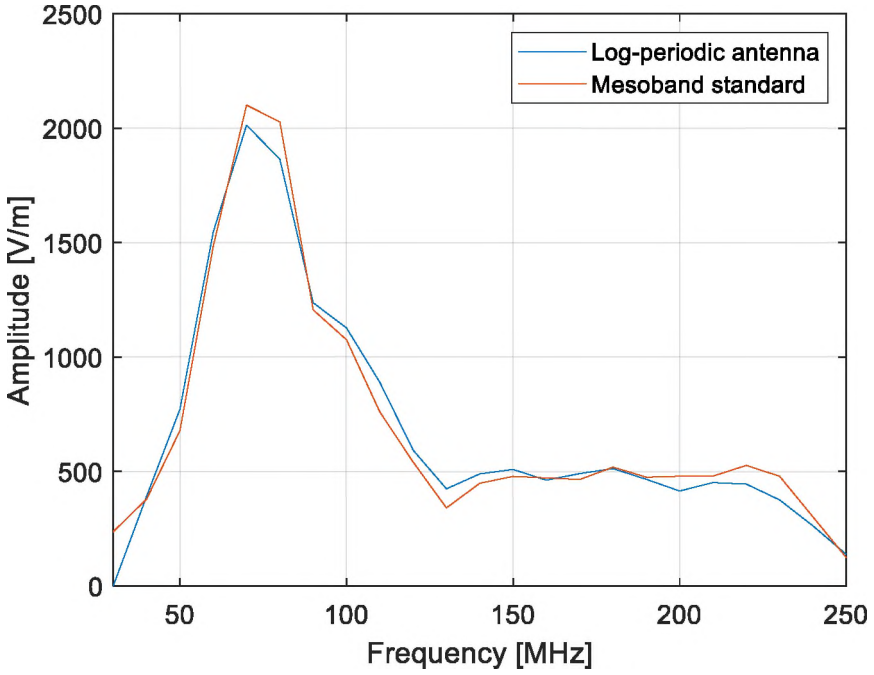

(a) Single side spectrums in the frequency domain

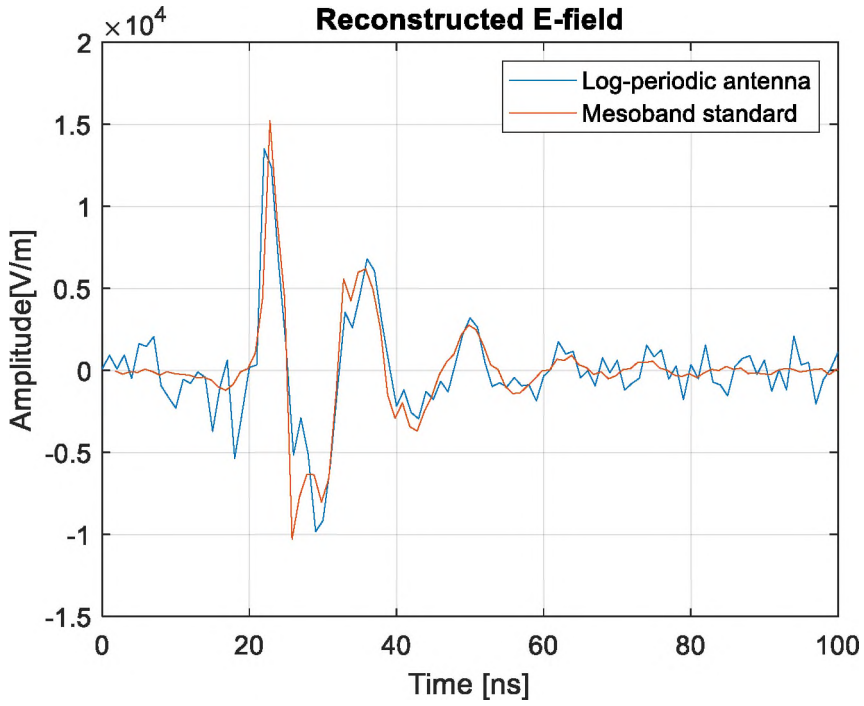

(b) Waveforms in the time domain

Figure 8. Comparison of the reconstructed and the measured electric fields E_z

The transfer function of the mesoband standard source measured using the TEM sensor was also calculated with the data in [2]. On the simulation, the unit dipole was set as a source in Figure 6 to extract the transfer function directly from the measured field. In Figure 7, the transfer function of the log- periodic antenna is similar to the other sources below 250 MHz. Due to the structure of the standard source generator mentioned above, the standard source generator is a dipole antenna, which has a length of 1.15 m. Since it operates as an open circuit when the wavelength is the same as the length of the dipole, it shows a null at 260 MHz.

To verify the transfer function of the log-periodic antenna, the electric field was regenerated with dipole moments of the standard source multiplied by the transfer function referring to (3) and it is compared with the measured electric field of the standard source as shown in Figure 8. The regenerated waveform matched well with the real standard source measurement. It shows that the transfer function of the log-periodic antenna is comparable to the transfer function of the standard source.

3. TRANSFER FUNCTION MEASUREMENT TO CHARACTERIZE AUTOMOTIVE IEMI

Most vehicles have ECUs, which are placed near the front center console. To check the IEMI effect to the ECU, the IEMI source is placed 5 m away from the front, rear, and side of the vehicle and the D-dot sensor is placed near the accelerator pedal to extract the transfer function between the attacker and the victim.

3.1. IEMI MEASUREMENT WITH THE LOG-PERIODIC ANTENNA

Figure 9 describes the IEMI measurement setup. The log-periodic antenna was placed as the IEMI source and the vehicle as the victim. Similar to in Section 2, two external amplifiers were added. The power amplifier was attached to the log-periodic antenna, and the preamplifier was attached to the output of the balun. Compared with the preamplifier, the power amplifier is used to amplify the power of a 0 - 10 dBm range. The D-dot sensor was placed near the accelerator pedal to measure the radiated electric

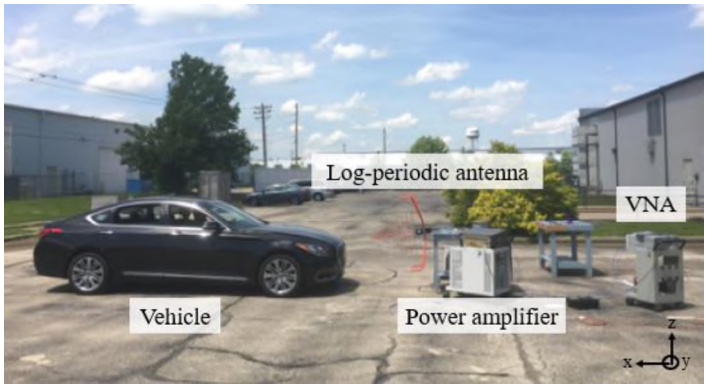

(a) Measurement setup with the vehicle

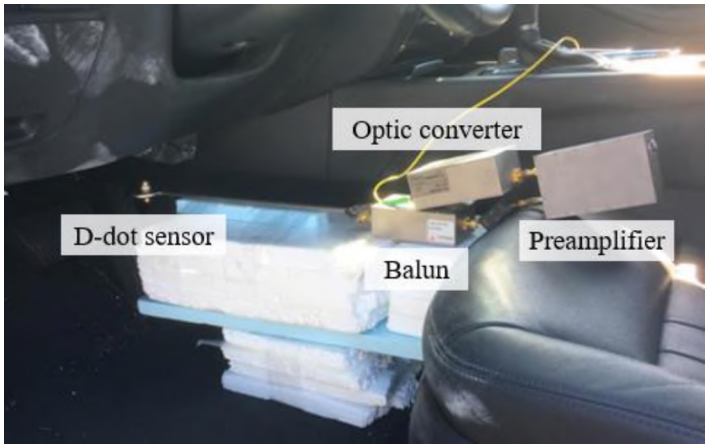

(b) D-dot sensor placement near the pedal

Figure 9. The IEMI measurement setup with the vehicle

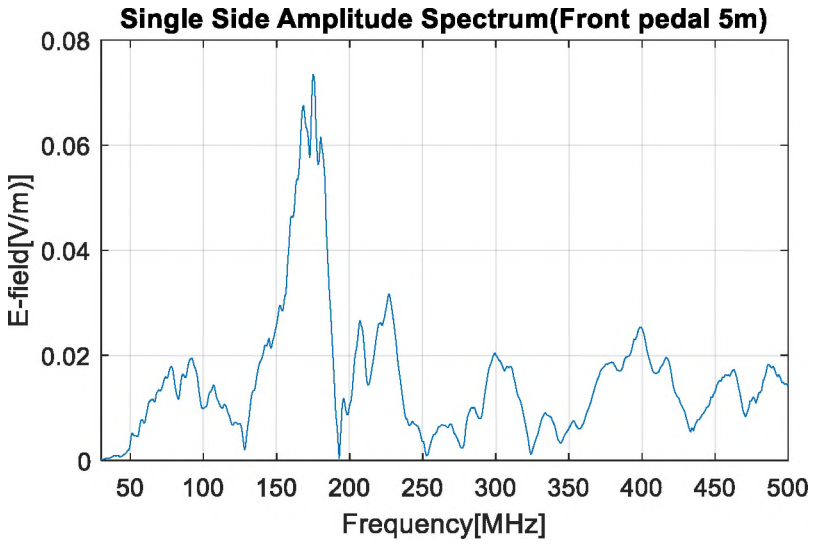

Figure 10. The electric field E_z at 5 m away from the source to the vehicle

field from the IEMI source since the pedal is near the front center console. Figure 10 shows the measured electric field E_z. To extract the transfer function, the electric field E_z was divided by the dipole moment P_z of the log-periodic antenna.

3.2. VALIDATION OF THE TRANSFER FUNCTION

The transfer functions of different IEMI sources with the vehicle 5 m away from the source to the front of the vehicle are extracted and compared as shown in Figure 11. Transfer functions of the log-periodic antenna and the standard source can be calculated by (3) with a measured electric field inside the vehicle.

To validate the transfer function of the log-periodic antenna with the vehicle, the electric field was regenerated with dipole moments of the standard source and compared with the real measurement of the standard source as Figure 12. The magnitude of the log-

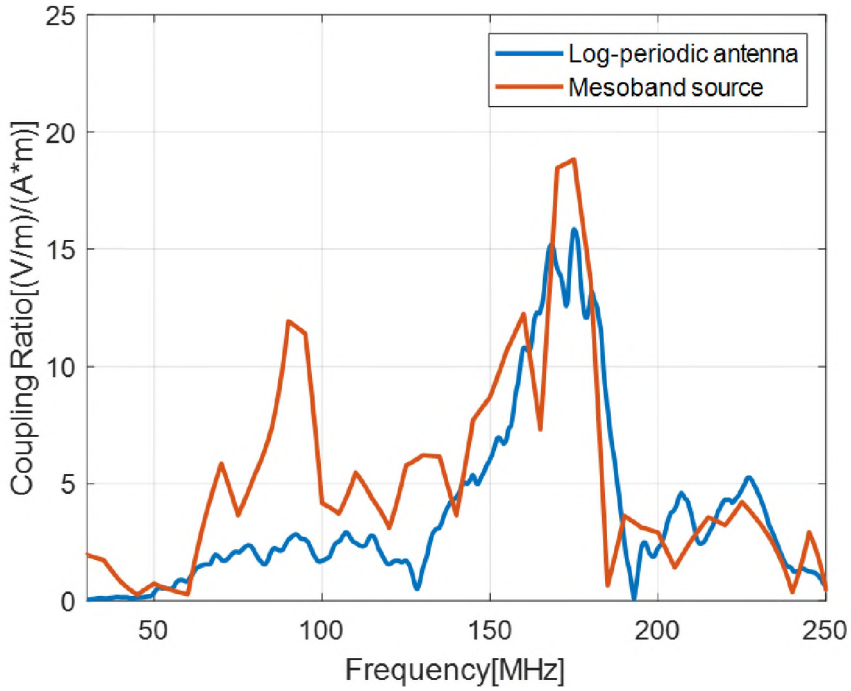

Figure 11. Transfer function comparison with the vehicle

periodic antenna at 50 – 100 MHz range is lower than the standard source due to the transfer function. Consequently, the main signal of the time domain waveform is 80 MHz and the magnitude of the log-periodic antenna is affected by the transfer function. Overall, the regenerated waveform in the time domain follows the same trend as the standard source, and it shows that the transfer function of the log-periodic antenna is comparable to the measurement of the standard source. Additionally, the victim was illuminated from the rear, and side. The measurement results show similar tendencies as the front and are not included in the manuscript.

To measure the field radiated from the standard IEMI source, an oscilloscope and the D-dot sensor was used. An oscilloscope has internal noise, and the noise floor level is related with the bandwidth as Equation (4) shown below:

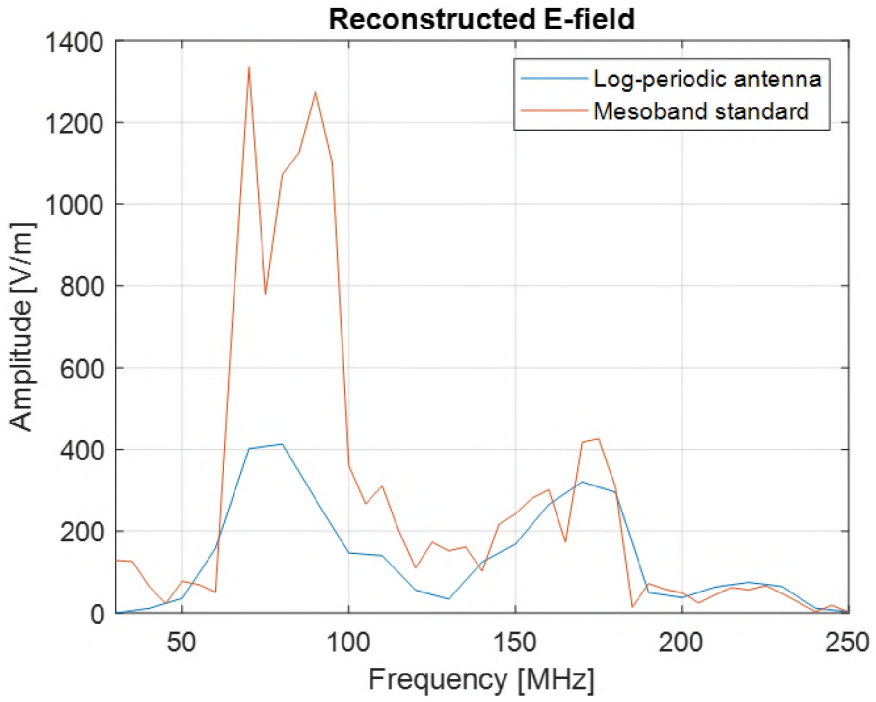

(a) Single side spectrums in the frequency domain

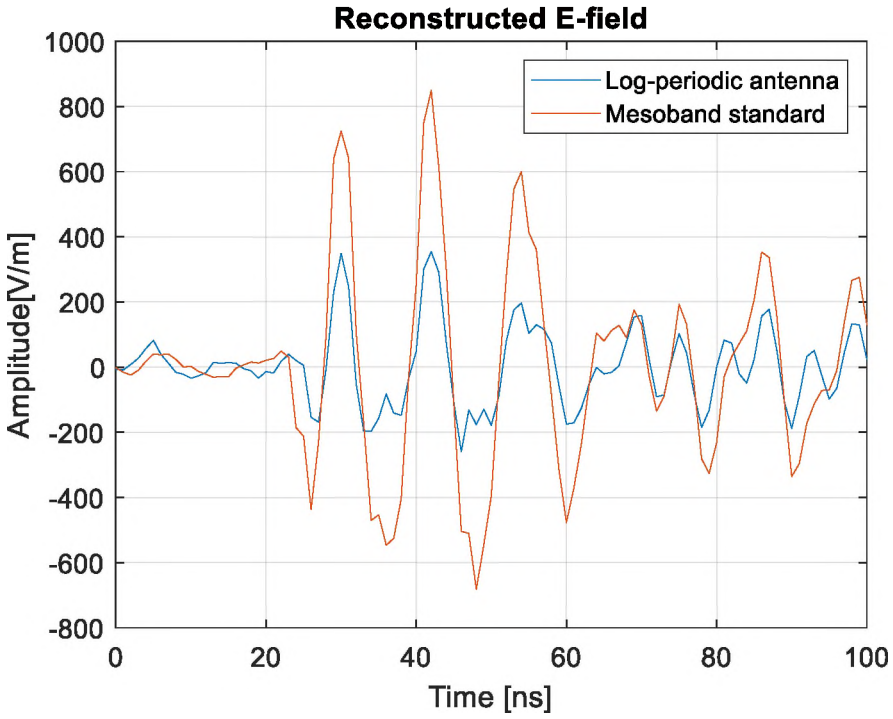

(b) Waveforms in the time domain

Figure 12. E-field comparison generated with different transfer functions

$$Noise\ floor\ [dBm] = -174 + Noise\ figure + 10\log\,(Bandwidth), \quad (4)$$

where the bandwidth indicates the range of frequencies that the oscilloscope can acquire and display accurately with less than 3 dB attenuation. As mentioned in Section 2, a D-dot sensor captures the time-derivative of the electric field; it has the jω term in the frequency domain. The output voltage of the D-dot sensor is divided by jω to get the electric field by (3), which is affected by the oscilloscope's noise in the low frequency region. However, there was not a similar trend of the mesoband standard source in Figure 8(a) below 50 MHz, since the TEM sensor was used to measure the field to characterize the standard source generator in Section 2. As the output of the TEM sensor is proportional to the electric field, it does not need to be divided by jω.

To verify the low frequency noise in the standard source measurement, the idle noise was measured using the D-dot sensor and the oscilloscope with the following

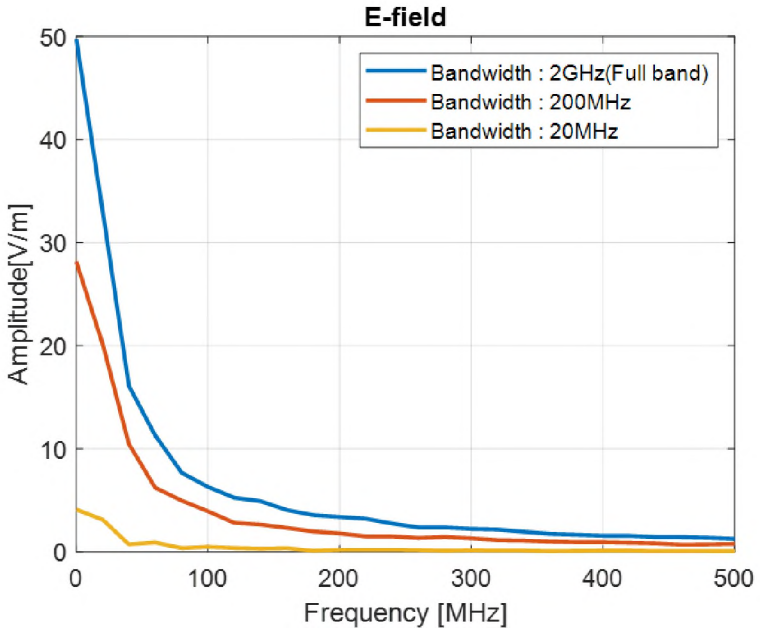

Figure 13. Idle noise measurement with different bandwidth settings

bandwidth settings: 2 GHz(full band), 200 MHz, and 20 MHz. Measured signals were converted to the electric field in the frequency domain as Figure 13. In the low frequency region, it is similar to the measurement data of the standard source in Figure 12(a). It shows that the low frequency noise is related with the internal noise of an oscilloscope and the characteristics of a D-dot sensor. This issue can be resolved by attaching an integrator after the D-dot sensor, using a vector network analyzer (VNA) or a spectrum analyzer.

4. CONCLUSION

Using a log-periodic antenna as an IEMI attacker, the transfer function between the aggressor and the ECU is extracted and compared with the mesoband standard source measurement. To validate the transfer function, the electric fields are reconstructed as the extracted transfer function multiplied by dipole moments of the standard source. It is found that the extracted transfer function of the log-periodic antenna is comparable to the transfer function of the standard source. It is expected that the transfer function measurement can be considered to analyze how the automotive IMEI affects the vehicle.

ACKNOWLEDGEMENTS

This work was supported in part by the National Science Foundation under Grant No. IIP-1916535.

REFERENCES

[1] P. O. Leach and M. B. Alexander, "Electronic Systems Failures and Anomalies Attributed to Electromagnetic Interference," NASA Report 1374, National Aeronautics and Space Administration. Washington, CC 20546-0001, July 1995.

[2] Y. Zhong, W. Song, C. Kim, C. Park and C. Hwang, "Intentional Electromagnetic Interference Source Reconstruction for Automotive Simulation," IEEE Asia-Pac. Electromagn. Compat. Symp, 2019.

[3] M. Bäckström, "HPM testing of a Car: A Representative Example of the Susceptibility of Civil Systems", 13th International Zurich Symposium Supplement, February 1999, pp. 189-190.

[4] Sabath, F., "What can be learned from documented Intentional Electromagnetic Interference (IEMI) attacks?" 2011 XXXth URSI General Assembly and Scientific Symposium, pp.1-4, 13-20 Aug. 2011.

[5] R. J. Spiegel, C. A. Booth, E. L. Bronaugh, "A Radiation Measuring System with Potential Automotive Under-Hood Application," IEEE Trans. Electromagn. Compat., vol. 25, pp. 61–69, May 1983.

[6] IEC 61000-4-36. Available: https://www.iec.ch/.

[7] C. A. Balanis, "Antenna Theory: Analysis and Design," 4th ed. Hoboken, NJ, USA: Wiley, 2016.

[8] L. Sangsu, Y. Zhong, Q. Huang, T. Enomoto, S. Seto, K. Araki, J. Fan, and C. Hwang. "Analytical Intra-system EMI Model Using Dipole Moments and Reciprocity." Proc. IEEE Asia-Pac. Electromagn. Compat. Symp, 2018.

[9] P. Wilson, "On correlating TEM cell and OATS emission measurements," IEEE Trans. Electromagn. Compat., vol. 37, no. 1, pp. 1–16, Feb. 1995.

II. THERMAL RUNAWAY INVESTIGATION OF LITHIUM-ION BATTERY BY INTENTIONAL EMI

Woncheol Song, Seungtaek Jeong, Jonghyun Park, and Chulsoon Hwang

ABSTRACT

Lithium-Ion (Li-ion) batteries are being widely used and many accidents related with Li-ion batteries are also increasing. For most battery applications, a voltage regulator module (VRM) is applied to regulate the voltage from the battery to its output, such as integrated circuits (ICs). A bypass capacitor at the input path of VRM is needed and the supply voltage after VRM can be stable to enable the operation of ICs with this bypass capacitor. Due to this bypass capacitor and the inductance at the battery side from wires or printed circuit board (PCB) traces, the parallel LC resonance can be generated and it resonates the current flowing through the battery. To mimic the electromagnetic environment which can affect the battery system inducing a current passing through the battery, the current is intentionally injected to the system with a bulk current injection (BCI) probe and it is investigated how this coupled current can affect the battery with this parallel LC resonance.

1. INTRODUCTION

Lithium-Ion (Li-ion) batteries are being widely used nowadays for electric vehicles and electric devices and the demand is rapidly growing. Also, they can be

applied for military and aerospace systems since they have high energy and power density, deliver more energy and power with less weight and maintenance than conventional batteries such as alkaline and Nickel Cadmium (Ni-Cd) [1]. However, many accidents related with Li-ion batteries have been reported recently, for example, Samsung Galaxy Note7 battery explosion as Figure 1, Boeing 787 Li-ion battery explosion as Figure 2.

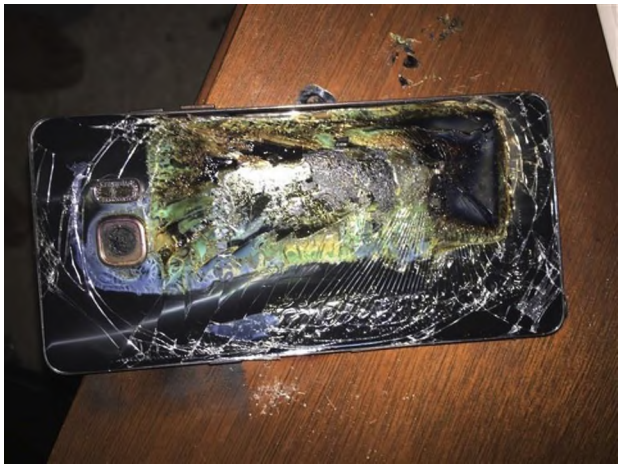

Figure 1. Samsung Galaxy Note7 battery explosion [2]

Figure 2. Boeing 787 Li-ion battery explosion [3]

For electromagnetic critical systems such as electric vehicles and aerospace systems which can affect the security of vehicle itself and also human lives, intentional electromagnetic interference (IEMI) is being considered as a growing threat and many researches have been done to investigate how IEMI affects vehicles [4-7]. Also, many vehicle manufacturers nowadays try to build their products lighter for energy efficiency and it reduces the need of metal or conductive materials but in perspective for shielding to the external electromagnetic fields, it makes worse since high-power electromagnetics (HPEM) radiated from IEMI attackers can increase the induced current through the wires.

For most battery applications, a voltage regulator module (VRM) is applied to regulate the voltage from the battery to its output, such as integrated circuits (ICs). With a VRM, ICs can operate with accurate drain voltages. Bypass capacitors at the input path of VRM are needed in electronics since a bypass capacitor supports that the supply voltage can be stable to enable the operation of ICs.

Due to this bypass capacitor and the wire inductance at the battery side, the parallel LC resonance is generated and it resonates the current flowing through the battery. When the frequency of the induced current by RF signal is same as the resonance frequency, the induced current can be amplified. This can be one possible scenario that the resonance affects a thermal runaway of the battery not due to the battery itself and it is investigated in this paper.

2. ELECTROMAGNETIC ENVIRONMENT CONSIDERATION

In IEC 61000-4-36 [8], IEMI source types are categorized and the 'specialist' generator can generate hundreds of kV and MV in terms of 'rE_{far}', the electric field normalized at a distance of 1 m from the antenna as derived from an electric field measurement at a given distance in the far field, and victims can be damaged permanently with tens or hundreds of kV/m electric fields as far as 50 m away from these generators [9].

Table 1. IEMI Source Type Categorized with Respect to Far Field Electric Field [8, 9]

Technical Category	IEMI Source Type	IEMI Technology Type	rE_{far} (V)
Novice	Hyperband	ESD gun	5 kV
	Hypoband	Microwave oven magnetron	2 kV
Skilled	Hyperband	Solid state pulsers	60 kV
	Mesoband	Commercially available pulser	120kV
	Hypoband	Typical radar	450kV
Specialist	Hyperband	Military demonstrator	~5 MV
	Mesoband	Military demonstrator	500 kV
	Hypoband	Military demonstrator	30 MV

In MIL-STD-464C [10], pulsed radar systems can generate high field strengths above 20 kV/m [11].

In RTCA DO-160G [12], the induced current by radiated RF fields from radio and radar transmitters are assumed to result in current levels up to 300 mA and these levels in Figure 3 are being considered for the conducted susceptibility test for aircraft.

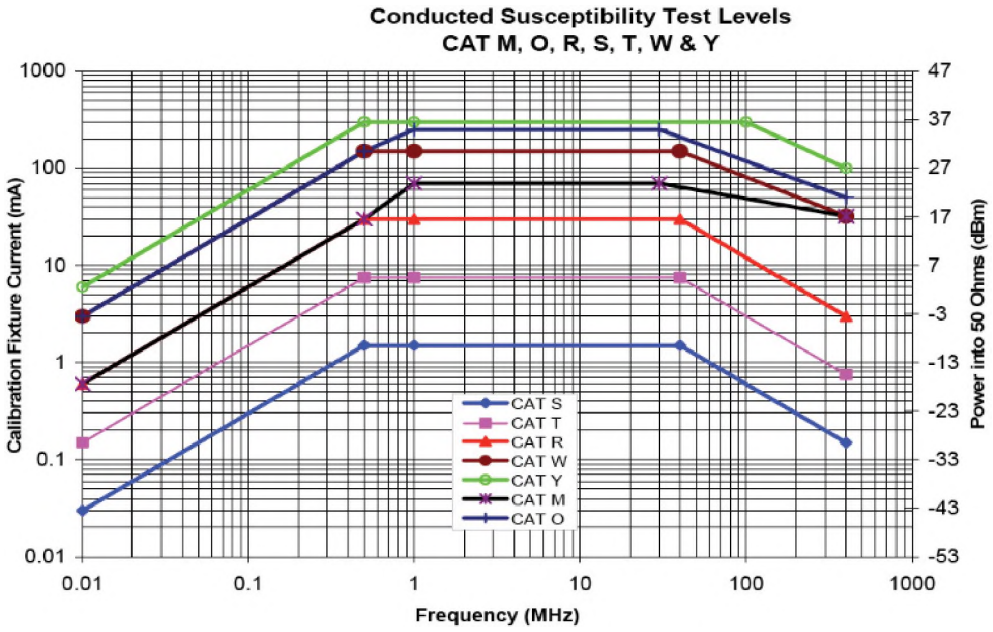

Figure 3. Conducted Susceptibility Current Limits [12]

In MIL-STD-461F [13], CS114, conducted susceptibility, bulk current injection test is explained and the injection level is limited up to 109 dBuA(same as 281.8 mA) for aircraft platform as Figure 4.

These indicate that the HPEM can induce hundreds of mA current for the worst case onto imperfectly shielded cables and this unwanted current can pass through batteries or other ICs which are connected to the cables directly and eventually can damage the system.

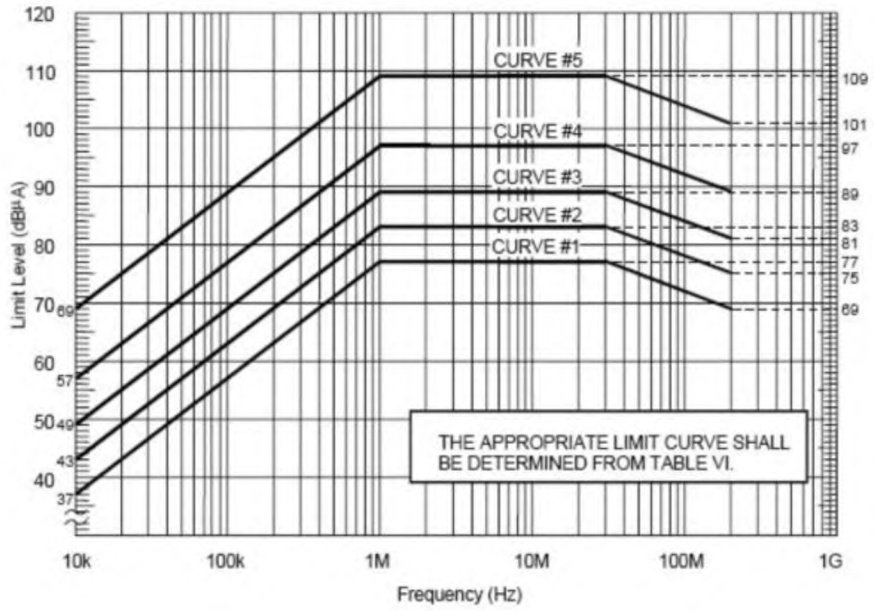

Figure 4. CS114 Injection Current Limits [13]

3. BULK CURRENT INJECTION TEST

To mimic this electromagnetic environment to inject a RF current in a wire, a bulk current injection (BCI) probe is used to inject a current intentionally. This BCI probe is modeled as an AC current source, which can be described as inductive coupling at the load. The equivalent circuit and the test setup are described in Figure 5. Each component is measured with a vector network analyzer (VNA). The battery has 100 nF capacitance and the wire connected to the battery consists of 400 nH inductance with 1.05 Ω DC resistance and 55.6 pF capacitance in parallel. The bypass capacitor is attached as 100 pF and the load is set as 100 Ω.

Considering the BCI probe as an AC current source, this parallel 400 nH and 100 pF acts as a tank resonant circuit and the current flowing through this circuit is resonated

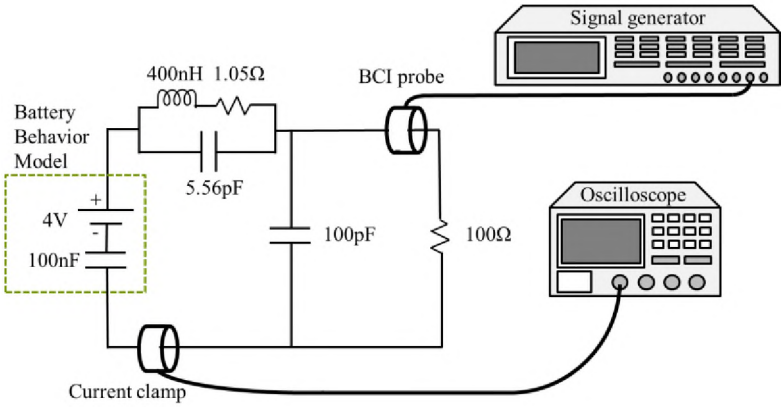

(a) The illustration of the setup and the equivalent circuit

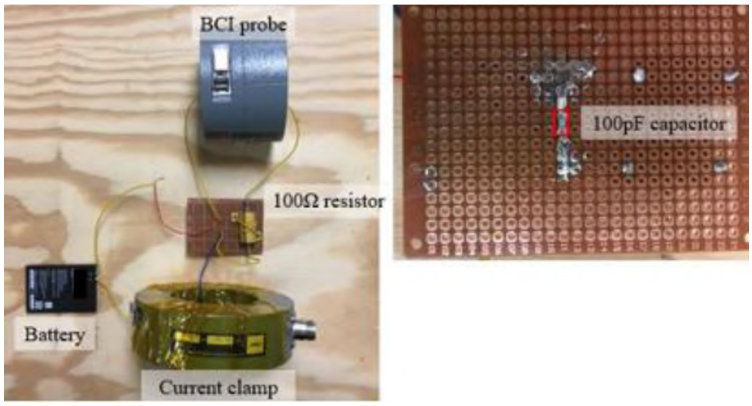

(b) The setup with the circuit attaching the battery

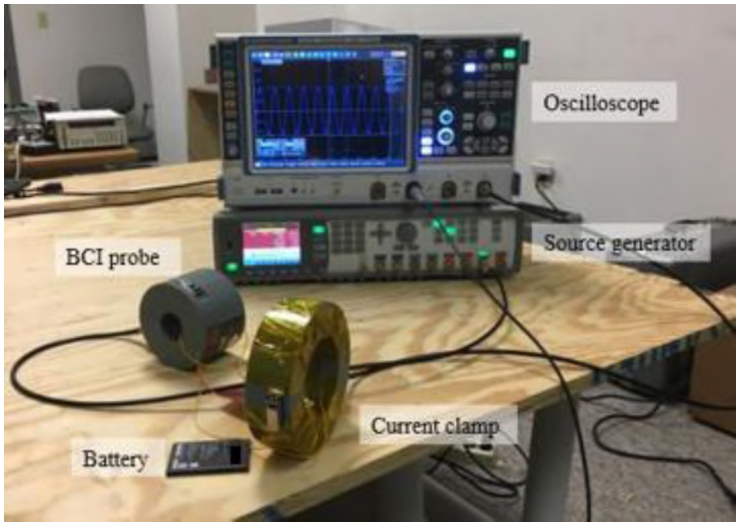

(c) The measurement setup description

Figure 5. BCI measurement setup

at the resonance frequency. To calculate the current gain passing through the battery, the input current is measured at 100 Ω load and the output current is measured at the battery with a current clamp. Compared with the simulation result of the equivalent circuit, the measurement matches well with the simulation below 30MHz as Figure 7.

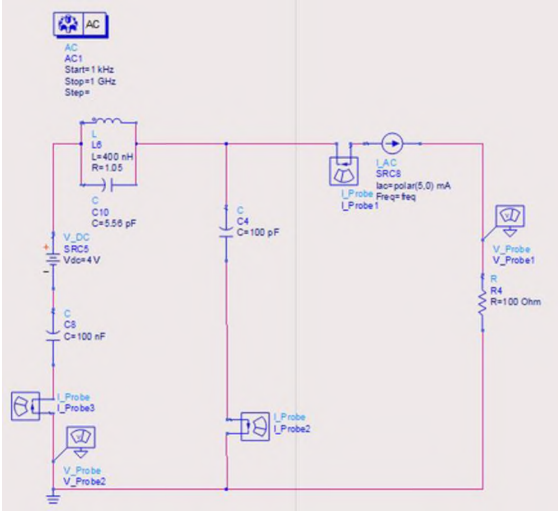

Figure 6. ADS circuit simulation for the current gain calculation

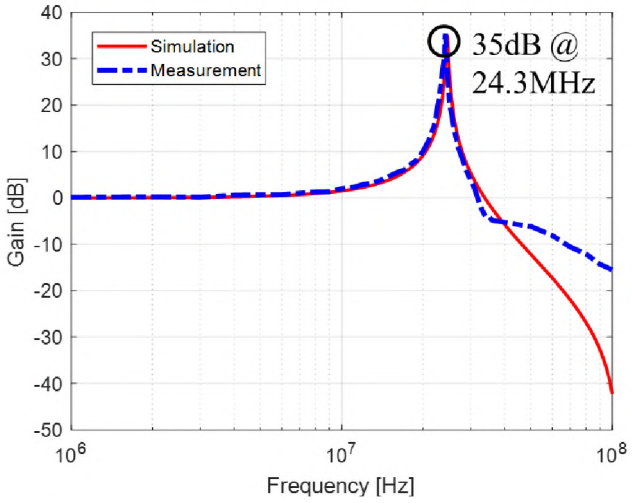

Figure 7. BCI current gain comparison

The measured resonance frequency is 24.3MHz and it matches well with the simulation, 24.5MHz. It indicates that the equivalent circuit including the behavior model of the battery is correct. The inductance of the battery side comes from the wire and this affects the parallel LC resonance with the bypass capacitor.

4. THERMAL RUNAWAY INVESTIGATION

The bulk current injection test is performed again with a power amplifier to inject higher current to the battery. With the test setup in Figure 8, 38.5 mA peak-to-peak (pp) current at 24.3 MHz is injected at the load as Figure 9(a). The current flowing through the battery is amplified to 2.17 A pp as Figure 9(b) by the parallel LC resonance.

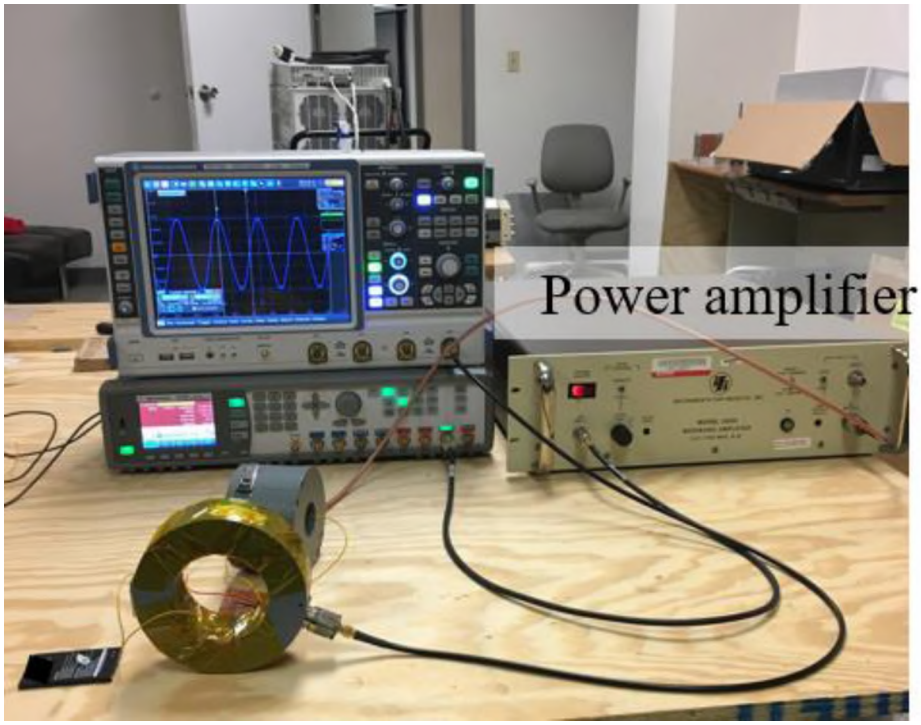

Figure 8. BCI measurement setup with a power amplifier

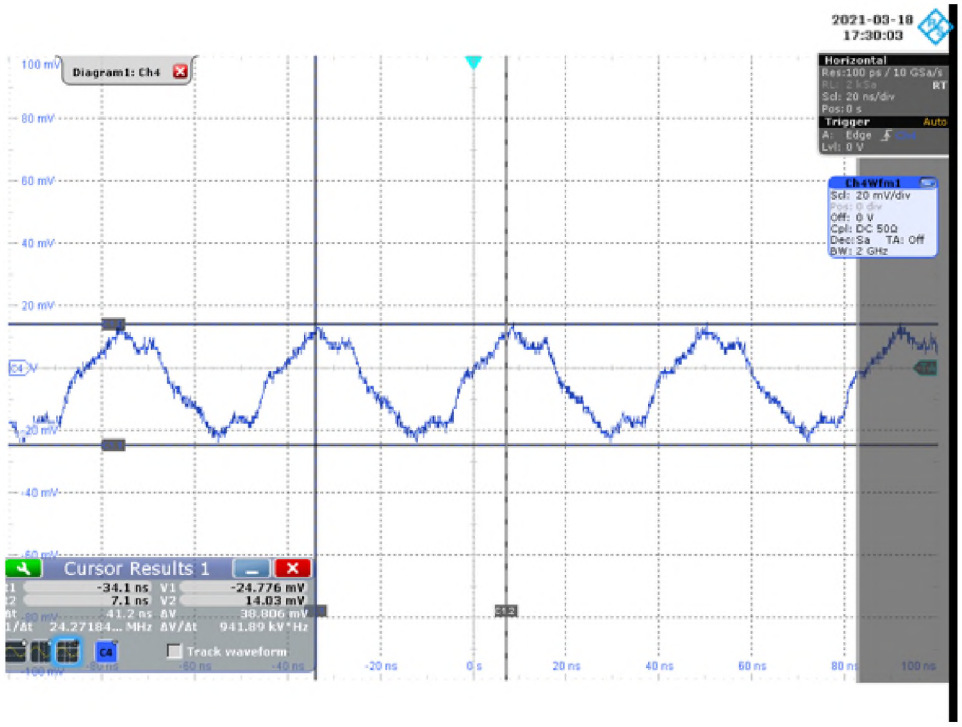

(a) The input current: 38.5 mA peak-to-peak measured at the 100 Ω load

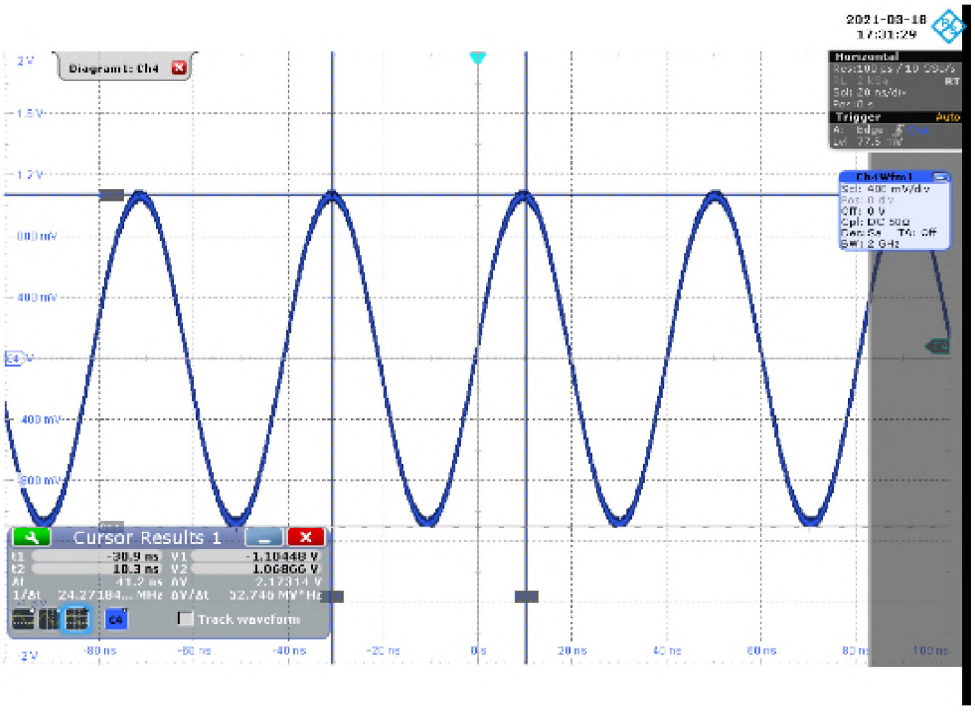

(b) The output current: 2.17 A peak-to-peak measured at the battery

Figure 9. Current measurement results at 24.3 MHz

To verify that the LC tank resonance affects the battery temperature, the temperature of the battery is measured with a thermal camera and compared with the temperature of the battery with the default setup. The default setup is that the battery is connected to the 100 Ω load but the current injection is disabled. With the default setup, the temperature of the battery is stable near 24 - 25 °C during 30 minute measurement. However, after enabling the current injection, the temperature is gradually increased from 24.6 °C to 29.6 °C after 30 minutes as Figure 11. Also, the heat is mostly focused on the battery's positive and negative terminals. It indicates that the heat is generated from the

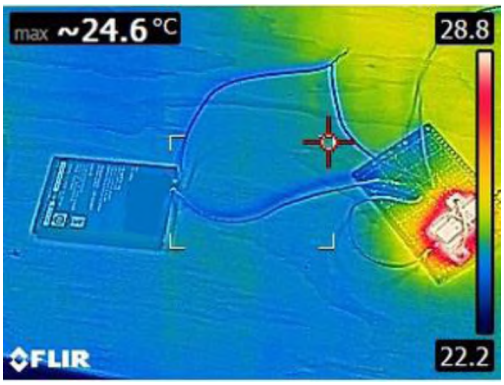

(a) The initial battery temperature

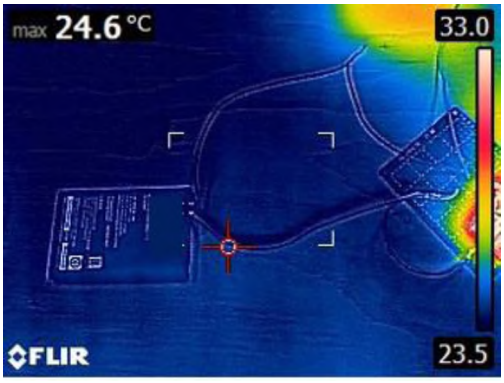

(b) The battery temperature after 30 minutes

Figure 10. The battery temperature measurement with 100Ω load

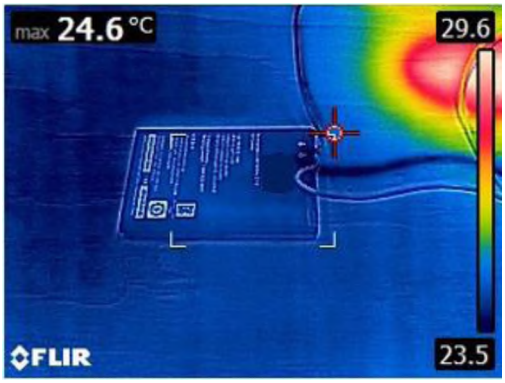

(a) The initial battery temperature

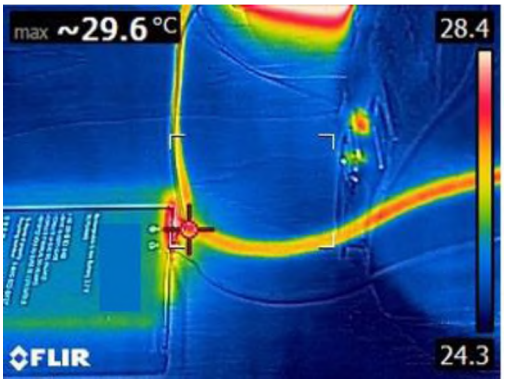

(b) The battery temperature after 30 minutes

Figure 11. The battery temperature with enabling the current injection

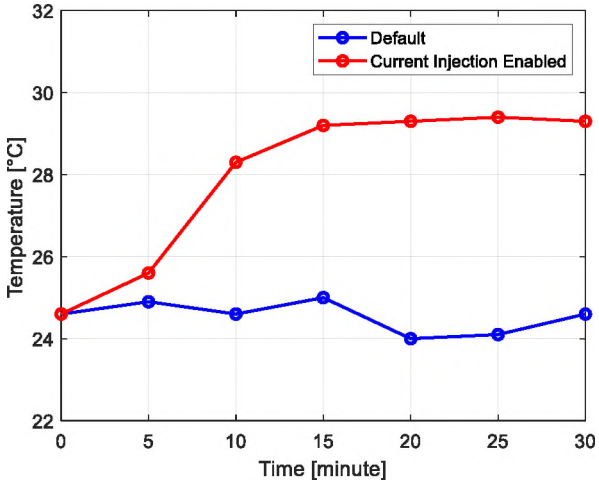

Figure 12. The battery temperature comparison

battery and the amplified current by the resonance affects the battery to increase the temperature since the current densities near two terminals are higher than others.

It is checked how the temperature is changed with different levels of current injection. As Figure 13, the temperature depends on the current injection level. It indicates that the injected current affects the battery to increase the temperature and the heat is generated due to the current injection.

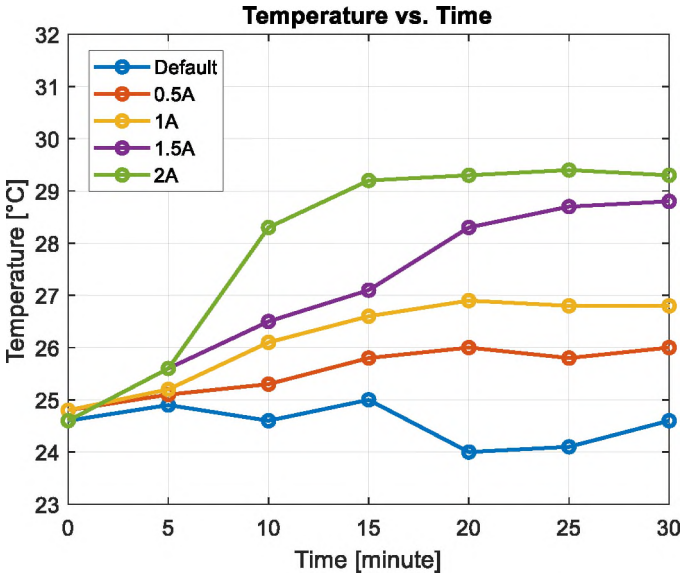

Figure 13. The battery temperature with different current injection levels

5. CONCLUSION

The current passing through the battery is amplified due to the parallel LC resonance from the bypass capacitor and the wire inductance of the battery side. By BCI test, the heat from the battery is generated and it is found that the temperature is affected by the current flowing through the battery. Most of battery applications need to use a

VRM so this resonance is inevitable. Most solutions of the thermal runaway of Li-ion batteries are focused on the battery itself. However, based on this measurement, it is found that currents induced by RF noises can be a reason that the thermal runaway is occured with the battery system. Engineers should recognize this situation and optimize the wire inductance of the battery side or the bypass capacitor values to prevent the thermal runaway by RF noises.

REFERENCES

[1] J. M. Kolly, J. Panagiotou, and B. A. Czech, The Investigation of a Lithium-Ion Battery Fire Onboard a Boeing 787 by the US National Transportation Safety Board. Dothan, AL, USA: Saf. Res. Corp.America, 2013, pp. 1–18.

[2] Website : https://www.nbcnews.com/tech/tech-news/samsung-finally-explains-galaxy-note-7-exploding-battery-mess-n710581.

[3] Website : https://en.wikipedia.org/wiki/Boeing_787_Dreamliner_battery_problems#/media/File:1-7-12_JAL787_APU_Battery.JPG.

[4] W. Song, Y. Zhong, C. Kim, C. Park and C. Hwang, "Transfer Function Measurement for Automotive Intentional Electromagnetic Interference", 2020 IEEE International Symposium on Electromagnetic Compatibility & Signal/Power Integrity (EMCSI), pp. 276-281, 2020.

[5] Y. Zhong, W. Song, C. Kim, C. Park, and C. Hwang, “Intentional Electromagnetic Interference Source Reconstruction for Automotive Simulation,” IEEE Asia-Pac. Electromagn. Compat. Symp, 2019.

[6] Y. Zhong, W. Song, C. Kim, C. Park, and C. Hwang, "Efficient automotive simulation using reciprocity for intentional electromagnetic interference", Proc. IEEE Int. Symp. Electromagn. Compat. Signal Power Integr., pp. 600-604, Jul. 2019.

[7] Y. Zhong, W. Song, C. Kim, and C. Hwang, "Coupling Path Visualization and Its Application in Preventing Electromagnetic Interference", IEEE Transactions on Electromagnetic Compatibility, vol. 62, no. 4, pp. 1485-1492, August 2020.

[8] IEC 61000-4-36. Available: https://www.iec.ch/.

[9] O, Izadi, R. Frazier, N. Altunyurt, S. Sedighsarvestani, D. Pommerenke, and C. Hwang, "A New Tunable Damped Sine-like Waveform Generator For IEMI Applications", 2020 IEEE International Symposium on Electromagnetic Compatibility & Signal/Power Integrity (EMCSI), 2020.

[10] MIL-STD-464C, ELECTROMAGNETIC ENVIRONMENTAL EFFECTS REQUIREMENTS FOR SYSTEMS, DEPARTMENT OF DEFENSE, 2010.

[11] E. Dubois, H. Kherbouchi, and J. Bosson, "Thermal Runaway of Lithium-Ion Batteries Triggered by Electromagnetic Interference", IEEE Transactions on Electromagnetic Compatibility, vol. 62, no. 5, pp. 2096-2100, October 2020.

[12] RTCA DO-160G, Environmental Conditions and Test Procedures for Airborne Equipment, RTCA Inc.

[13] MIL-STD-461F, Requireemnts for The Control of Electromagnetic Interference Characteristics of Subsystems and Equipment, Department of Defense, 2007

SECTION

2. CONCLUSIONS

In the first paper, using a log-periodic antenna as an IEMI attacker, the transfer function between the aggressor and the ECU is extracted and compared with the mesoband standard source measurement. To validate the transfer function, the electric fields are reconstructed as the extracted transfer function multiplied by dipole moments of the standard source. It is found that the extracted transfer function of the log-periodic antenna is comparable to the transfer function of the standard source.

In the second paper, the heat from the battery is generated by BCI test and it is found that it is due to the parallel LC resonance from the bypass capacitor and the wire inductance of the battery side. Most of the battery application needs to use a VRM so this resonance is inevitable. To prevent this situation, the wire inductance of the battery side or the bypass capacitor values should be optimized to prevent the thermal runaway by RF noises with considering their frequencies.

VITA

Woncheol Song received his B.S. degree in Electronics Engineering from Konkuk University, South Korea in February 2015. He received his M.S. degree in Electgrical Engineering from Missouri University of Science and Technology in July, 2021. He joined the EMC laboratory as a graduate research assistant from August 2018 to May 2021. He was a Hardware Engineer with Mobile Communications Company, LG Electronics, Inc., Seoul, South Korea, from January 2015 to July 2018. Also, he was a co-op Hardware Engineer with Enterprise Access Switching team, Cisco Systems, Inc. from August 2019 to July 2020.